12-1-2023

Metal organic frameworks with carbon black for the enhanced electrochemical detection of 2,4,6-trinitrotoluene

Shaghraf Javaid

Muhammad R. Azhar
Edith Cowan University

Xinyu Li

Juliette I. Phillips

Tanveer Hussain

See next page for additional authors

10.1016/j.mtchem.2023.101759
Javaid, S., Azhar, M. R., Li, X., Phillips, J. I., Hussain, T., Abid, H., . . . Silvester, D. S. (2023). Metal organic frameworks with carbon black for the enhanced electrochemical detection of 2,4,6-trinitrotoluene. Materials Today Chemistry, 34, article 101759. https://doi.org/10.1016/j.mtchem.2023.101759

Materials Today Chemistry 34 (2023) 101759

Contents lists available at ScienceDirect

Materials Today Chemistry

journal homepage: www.journals.elsevier.com/materials-today-chemistry/

Metal organic frameworks with carbon black for the enhanced electrochemical detection of 2,4,6-trinitrotoluene

Shaghraf Javaid [a], Muhammad Rizwan Azhar [b], Xinyu Li [a], Juliette I. Phillips [a], Tanveer Hussain [c], Hussein Abid [b], Jun Chen [d], Xiaobo Ji [d], Debbie S. Silvester [a,*]

[a] School of Molecular and Life Sciences, Curtin University, GPO Box U1987, Perth, Western Australia, 6845, Australia
[b] School of Engineering, Edith Cowan University, 270 Joondalup Drive, Joondalup, Western Australia, Australia
[c] School of Science and Technology, University of New England, Armidale, NSW, 2351, Australia
[d] State Key Laboratory of Powder Metallurgy, College of Chemistry and Chemical Engineering, Central South University, Changsha, 410083, China

ARTICLE INFO

Keywords:
Electrochemistry
Sensing
2,4,6-Trinitrotoluene
Metal organic frameworks
Zn(BDC)
Solvent modulation
Hydrothermal

ABSTRACT

The sensing of explosives such as 2,4,6-trinitrotoluene (TNT) directly at an explosion site requires a fast, simple and sensitive detection method, to which electrochemical techniques are well suited. Herein, we report an electrochemical sensor material for TNT based on an ammonium hydroxide (NH_4OH) sensitized zinc-1,4–benzenedicarboxylate Zn(BDC) metal organic framework (MOF) mixed with carbon black on a glassy carbon electrode. In the solvent modulation mechanism, by merely changing the concentration of NH_4OH during synthesis, two Zn(BDC) MOFs with novel morphologies were fabricated *via* a hydrothermal approach. The as-prepared MOFs were characterized using X-ray powder diffraction (XRD), scanning electron microscopy (SEM), Fourier transform infrared (FTIR) spectroscopy, X-ray photoelectron spectroscopy (XPS) and high-resolution field emission electron microscopy (FESEM) equipped with energy dispersive X-ray spectroscopy (EDS). The different morphologies of the MOFs, and their impact on the performance of the modified electrodes towards the electrochemical detection of TNT was investigated. Under optimum conditions, 0.7–Zn(BDC) demonstrated the best electrochemical response for TNT detection using square wave voltammetry (SWV) with a linear calibration response in the range of 0.3–1.0 μM, a limit of detection (LOD) of 0.042 μM, a limit of quantification (LOQ) of 0.14 μM and a high rate of repeatability. Atomic-scale simulations based on density functional theory authenticated the efficient sensing properties of Zn(BDC) MOF towards TNT. Furthermore, the promising response of the sensors in real sample matrices (tap water and wastewater) was demonstrated, opening new avenues towards the real-time detection of TNT in real environmental samples.

1. Introduction

Nitroaromatic compounds (NACs) are widely used in modern military explosives and are popular in the fireworks and aviation industries. However, the frequent use and chemical nature of nitro-based compounds leads to the formation of persistent environmental pollutants in soil and water, especially close to explosion sites and ammunition storage areas [1]. NACs are mutagenic and carcinogenic, meaning that prolonged exposure can pose serious threats to human health, including skin irritation, anaemia and liver abnormalities [2]. Among several NACs that are available, 2,4,6–trinitrotoluene (TNT) is one of the most widely used compounds because it undergoes rapid pressurization and decomposition and is designed to detonate under specific temperature and pressure conditions acquired through primary explosives [3]. TNT is toxic to humans at concentrations above 2 parts-per-million (ppm) and its upper advisory level in drinking water is 2 parts-per-billion (ppb) [4]. Based on its prevalence in the demolition and mining industries, the swift and accurate detection of TNT is imperative for environmental protection. Its detection is also important for national security e.g. if the explosive gets into the wrong hands. To attend these demands, there is a requirement for a sensing device for TNT with ideal properties that allows it to be miniaturized, portable, accurate and require simple sample preparation and measurement methods. Electrochemical techniques are highly suitable for this purpose [5–7].

The unique electrochemical reduction of TNT shows three distinct voltammetric peaks corresponding to the reduction of the three nitro

* Corresponding author.
E-mail address: d.silvester-dean@curtin.edu.au (D.S. Silvester).

https://doi.org/10.1016/j.mtchem.2023.101759
Received 6 December 2022; Received in revised form 4 August 2023; Accepted 1 October 2023
Available online 23 October 2023

groups, and its mechanism has been widely explored and well-characterised in aqueous solutions. The generally accepted mechanism involves 6 electrons and 6 protons for each step, a total of 18 electrons, 18 protons [8]. A range of electrochemical methods have been employed for TNT detection in water, including measuring the current, voltage, impedance, conductivity and membrane potential at different concentrations of TNT [9]. Most often, the detection of TNT is carried out by combining a chemically selective layer with an electrochemical transducer [9].

In recent years, many active materials have been used as modified electrodes for the electrochemical sensing of TNT, including carbon nanotubes, graphene, and noble metal-based nanomaterials [7,10,11]. However, there is limited literature on the electrochemical sensing of TNT using metal organic framework (MOF) structures [12,13]. Metal organic frameworks (MOFs) are new class of 3D functional material that comprise of metals connected by an organic linker. They exhibit excellent textural properties with ultra-high surface area, regular porosity and an abundance of functional groups. To date, hundreds of MOFs have been synthesized and used in a range of applications including gas adsorption, gas separation, sensors, liquid phase adsorption and in photocatalysis [14–19]. MOFs are also used as a template for the further synthesis of metal oxides, nitrides and composites through calcination, which requires heat-intensive treatments at temperatures of ca. 500–580 °C [20]. The incorporation of an expensive noble metal such as gold or silver into MOFs has displayed encouraging electrochemical sensing performance for the detection of nitrobenzene [21]. However, it should be noted that even though the MOF precursors are themselves low cost, the use of gold and silver salts make these materials cost-prohibitive for scale-up.

Several MOFs have been used for the detection of gases [22], water pollutants [23], biological species [24,25] and nerve agents [26]. Among those, only a few have been used as synthesized in the pristine state, e.g. HKUST-1 for sensing of hydrogen [17], 2,4-dichlorophenol (DCP) [27], dopamine and pharmaceuticals [28,29]. To detect analytes using pristine MOFs as the electrode material, the MOF can be electrodeposited directly onto the electrode, such as in the case of HKUST-1. However, there are only a limited number of MOFs that can be electrodeposited in this way, but there are many more MOFs with different properties that can be produced in powder form. With this in mind, the current work examines the use of MOFs synthesized by hydrothermal methods with highly favourable inherent properties for the electrochemical detection of TNT. A Zn(BDC) MOF (where BDC = benzene dicarboxylic acid) was selected due to its facile synthesis technique, large surface area, and well-defined porosity. To achieve high stability of the sensing signal, and to tune the morphological aspects of the selected MOF for the sensing application, the synthesis is modified by adding ammonium hydroxide (NH_4OH) as a modulating solvent, leading to the formation of different flake-like morphologies. Two different volumes of NH_4OH (0.4 and 0.7 mL) are introduced into the synthesis of Zn(BDC). The electrochemical sensing of TNT is conducted by using Zn(BDC) MOFs in a paste together with carbon black and Nafion as modified glassy carbon electrodes (GCEs). Various parameters, including the analyte solution pH, TNT concentration and waiting times are studied to elucidate performance of the Zn(BDC) MOFs for the detection of TNT in both simulated and real samples. First principles calculations based on spin-polarized density functional theory (DFT) are performed to reveal the exchange and correlation functional and the electron-ion interactions. This study provides a foundation to explore pristine MOFs without costly noble metals for their highly favourable performance in electrochemical sensing applications.

2. Materials and methods

2.1. Chemicals and solutions

Zinc nitrate hexahydrate ($Zn(NO_3)_2.6H_2O$, 98 %), benzene dicarboxylic acid (BDC, $C_6H_4(CO_2H)_2$, 98 %), dimethylformamide (DMF, $HCON(CH_3)_2$, 99.8 %), ammonium hydroxide (NH_4OH, 29 wt% ammonia), sodium sulphate (Na_2SO_4, ≥99 %), boric acid (H_3BO_3, ≥99.5 %), sodium tetraborate decahydrate ($Na_2B_4O_7.10H_2O$, ≥99.5 %) and Nafion (~5 % in a mixture of lower aliphatic alcohols and water) were purchased from Sigma Aldrich, Australia, and used as received without any further purification. 2,4,6-Trinitrotoluene (TNT, 1000 μg/mL in acetonitrile) was purchased from Cerilliant Corporation, Round Rock, TX, USA. For electrochemical measurements, 0.5 M borate buffered Na_2SO_4 solution was used as a supporting electrolyte to prepare a 0.044 mM TNT solution. The prepared TNT solutions were stored in a refrigerator. Ultrapure water (with a resistance of 18.2 MΩ cm) was prepared by an ultrapure water purification system (Millipore Pty Ltd., North Ryde, NSW, Australia). For preparation of the slurry for drop casting on the electrode, super P carbon from Alfa Aesar (Thermo Fisher Scientific) was used, along with Nafion, ethanol and the MOF (see later).

2.2. Synthesis of 0.4–NH_4OH modulated Zn(BDC) MOFs

All MOF samples were synthesized using the hydrothermal method. First, 60 mL of DMF was heated to 100 °C for 2 h followed by adding 2.5 g of $Zn(NO_3)_2.6H_2O$ and 0.53 g of BDC. After continuous stirring for 30 min, 0.4 mL of NH_4OH was added to the reaction mixture. The solution was then transferred into a 120 mL capacity Teflon lined autoclave which was tightly sealed and kept at 130 °C in a preheated oven for 24 h before leaving it to cool to room temperature. The white crystalline product was isolated through vacuum filtration and left to dry at 100 °C for 12 h. The material is termed 0.4–Zn(BDC) in this work, reflecting the volume of NH_4OH (0.4 mL) added in the synthesis.

2.3. Synthesis of 0.7–NH_4OH modulated Zn(BDC) MOFs

The synthesis procedure for 0.7–NH_4OH modulated Zn(BDC) was similar to above, except that 0.7 mL of NH_4OH was added into the zinc precursor solution. This material has been given the name 0.7–Zn(BDC) in this work.

2.4. Preparation of Zn(BDC) modified GCE

A glassy carbon electrode (GCE, d = 3 mm, BASi, West Lafayette, IN, USA) was polished with 3, 1 and 0.5 μm alumina slurry (Kemet, NSW, Australia), followed by ultrasonication in ultrapure water and ethanol separately for 5 min. Before modifying the surface of the GCE, a cocktail of active material was prepared by mixing 5 mg of the Zn(BDC) MOF, 3 mg of carbon black, 50 μL of Nafion and 450 μL of ethanol. The cocktail was then sonicated for 60 min at room temperature. To prepare the Zn (BDC) modified electrode, 10 μL of the aforementioned cocktail was drop-casted onto the surface of a polished GCE and left to dry, yielding a robust electroactive surface denoted as either 0.4–Zn(BDC) or 0.7–(BDC) modified GCE. The modified GCEs were stored at room temperature. It is noted that carbon black was required to enhance the conductivity and improve the stability of the modified electrode. Films made with only MOF/Nafion (without carbon black) were non-homogeneous and gave irreproducible electrochemical results.

2.5. Electrochemical experiments

All electrochemical experiments were performed using a conventional three electrode system with a PGSTAT101 Autolab potentiostat (Metrohm Australia, Gladesville, NSW, Australia) interfaced to a PC system with NOVA 1.11 software. Experiments were performed at room temperature inside an aluminium Faraday cage to minimize electrical interference. The glassy carbon electrode, Pt mesh and Ag/AgCl (in saturated KCl, purchased from BASi) served as working, counter and reference electrodes, respectively. Prior to performing electrochemical experiments, the electrochemical cell was purged with high purity N_2 for

at least 15 min to remove any dissolved oxygen.

For the sensing experiments, cyclic voltammetry (CV) was performed at a scan rate (ν) of 100 mVs^{-1}, step potential of 2.44 mV, potential window between +0.1 and −1.0 V in a 0.5 M borate buffered Na_2SO_4 solution containing TNT. The pH of the electrolyte solution was adjusted carefully to 7 by using 99.5 % of H_3BO_3 and $Na_2B_4O_7$, respectively. To investigate the stability, repeatability and recovery of the modified electrodes, CV measurements were obtained with 20 or 60 min wait between each scan. Square wave voltammetry (SWV) was used to identify the linear calibration range with different concentrations of TNT because of its high sensitivity compared to CV. Parameters used for SWV were: $\nu = 40$ mV/s^{-1}, step potential = 4 mV, amplitude = 0.05 V and frequency = 10 Hz.

2.6. Effect of pH

To understand the influence of pH on the electrochemical reduction of TNT in aqueous media, three electrochemical measurements were carried out on the 0.7–NH_4OH modified GCE. All other experimental parameters were kept the same, except the pH of the supporting electrolyte (borate buffered Na_2SO_4 solution) which was either acidic (pH 4), neutral (pH 7) or basic (pH 9) to cover a wide range of pHs that mimics real water samples.

2.7. Wastewater and tap water

To determine the suitability of the prepared electrodes in real samples, spiked tap water and wastewater samples were analysed to detect TNT. Tap water was collected from the Chemistry & Resources Precinct at Curtin University, Perth, WA, Australia, and wastewater was collected from a local water source at Write Lake, Camillo, Western Australia.

2.8. Materials characterization techniques

A spectrum 100-FT-IR (Fourier transform infrared) spectrometer (PerkinElmer) was used to study the linkage of metal clusters with organic ligands. The spectra were scanned from 650 to 4000 cm^{-1} with a resolution of 4 cm^{-1} using an attenuated total reflectance (ATR) technique. Structural characterization of both the 0.4–NH_4OH and 0.7–NH_4OH modulated Zn(BDC) powders was performed using a D8 Advance diffractometer (40 kV/40 mA, Bruker AXS, Germany) with Cu – Kα radiation and a LynxEye detector to collect the X–ray diffraction (XRD) pattern. The MOF samples were scanned in a 2θ range of 20–80° with a 0.03 step size. N_2 adsorption/desorption isotherms of the samples were performed on a surface area and porosity analyser (Micromritics Tristar Plus 3020). All samples were degassed under vacuum at 5–10 torr in a quartz sample tube reactor at 160 °C for 24 h prior to measurements. Morphological features of the MOFs were investigated by recording scanning electron microscope (SEM) images from a Zeiss Neon 40EsB (Zeiss, Germany) instrument. High-resolution field emission scanning electron microscopy (FE-SEM, TESCAN MIRA3 LMU) equipped with an energy dispersive X-ray (EDX) spectrometer. Both machines were available at the John de Laeter Centre, Curtin University. Before imaging, the MOF samples were positioned onto carbon tape and coated with a 3 nm thick Pt layer. To investigate surface changes, X-ray photoelectron spectroscopy (XPS) (PHI 5000 Versaprobe III) measurements were performed with Al Kα (1486.6 eV) radiation operated at 72 W (12 kV, 6 mA) in a vacuum chamber at $\sim 2 \times 10^{-7}$ mbar pressure. The terms Zn(BDC) and Zn/GCE are used to indicate as-synthesized MOF, and the MOF modified electrode, respectively.

3. Results and discussion

3.1. Synthesis and modification of Zn(BDC)

Zn(BDC) MOFs were synthesized by conventional hydrothermal methods using different amounts of NH_4OH as a modulator. Two Zn (BDC) MOFs were prepared by adding either 0.4 or 0.7 mL of NH_4OH into the precursor solution. The use of modulators in such synthetic processes provides hindrance to the organic linkers and metal ions during the synthesis of MOFs, which can lead to controlled crystal growth and extension of the MOF [30]. Increasing the basicity of the solution by the addition of NH_4OH could also increase the availability of deprotonated BDC ions for coordination with zinc ions, thus producing more well-defined structures [31]. Therefore, it is generally agreed that adding NH_4OH as a modulator has a significant influence on the morphology, predominantly producing layered thin sheets and flake-like structures [32]. Keeping this in mind, the inspiration behind using this modulation technique was to take control over the morphology, porosity and surface area of the synthesized Zn(BDC) MOFs, and investigate the impact towards the electrochemical sensing of TNT. The as-synthesized MOFs were employed as an active material to prepare MOF-modified GCEs for the electrochemical detection of TNT. Fig. 1 presents a schematic of the MOF-modified GCE (bottom right), the structure of the MOF (top right), the electrochemical reduction mechanism (top left) and cyclic voltammetry for TNT reduction (bottom left).

For an in-depth understanding of the structural and morphological aspects of the synthesized MOFs, a range of characterization tests were performed. FTIR analysis showed the successful linkage of the zinc nodes with benzene dicarboxylic acid linkers. The main peaks in the FTIR spectra (Fig. 2a) are observed at 1368, 1575, 742, 3206 and 3602 cm^{-1}, corresponding to C═O, O–C–O, Zn–O, and –OH groups, respectively. To study the crystallinity, XRD patterns for pristine Zn(BDC), 0.4–Zn(BDC) and 0.7–Zn(BDC) were recorded (see Fig. 2b), which displayed characteristic reflections at 5, 10, 14 and 16° that are in fair agreement with the simulated XRD pattern of Zn(BDC). There are two additional peaks for 0.7–Zn(BDC), one extra peak for 0.4-Zn(BDC), and no peaks for Zn(BDC) between 5 and 10°, which may be a result of different space groups (*C*2/*c*, *P*2_1/*m*, and P21/C) for the same crystal structure [33]. Moreover, the intensity of 0.7–Zn(BDC) is higher compared to both the pristine and 0.4–Zn(BDC). Hence, the similarity and high crystallinity between the XRD pattern of both the 0.4–Zn(BDC) and 0.7–Zn(BDC) MOFs suggests that the addition of the modulator merely changes its morphology and not its core crystalline structure [21,34,35].

For a morphological understanding, SEM imaging was performed on

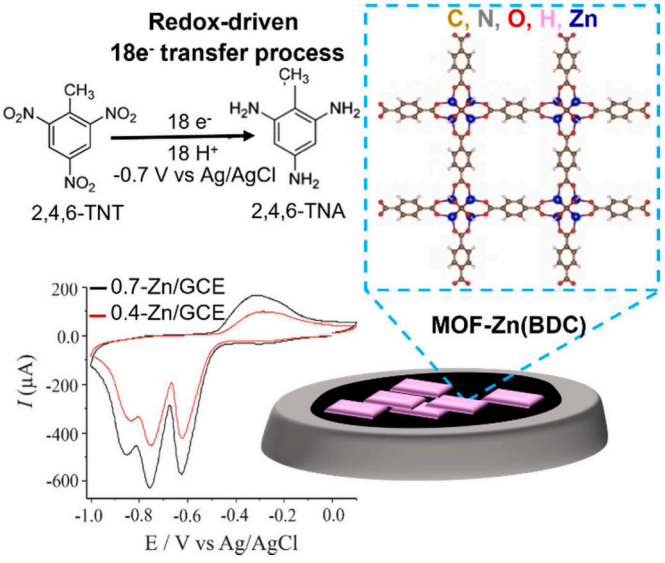

Fig. 1. Schematic illustration of the proposed mechanism for the electrochemical reduction of TNT on a 0.7-Zn/GCE modified electrode in an aqueous solution. Cyclic voltammetry was performed for 0.04 mM TNT in 0.5 M borate buffered Na_2SO_4 electrolyte at a scan rate of 100 mVs^{-1}.

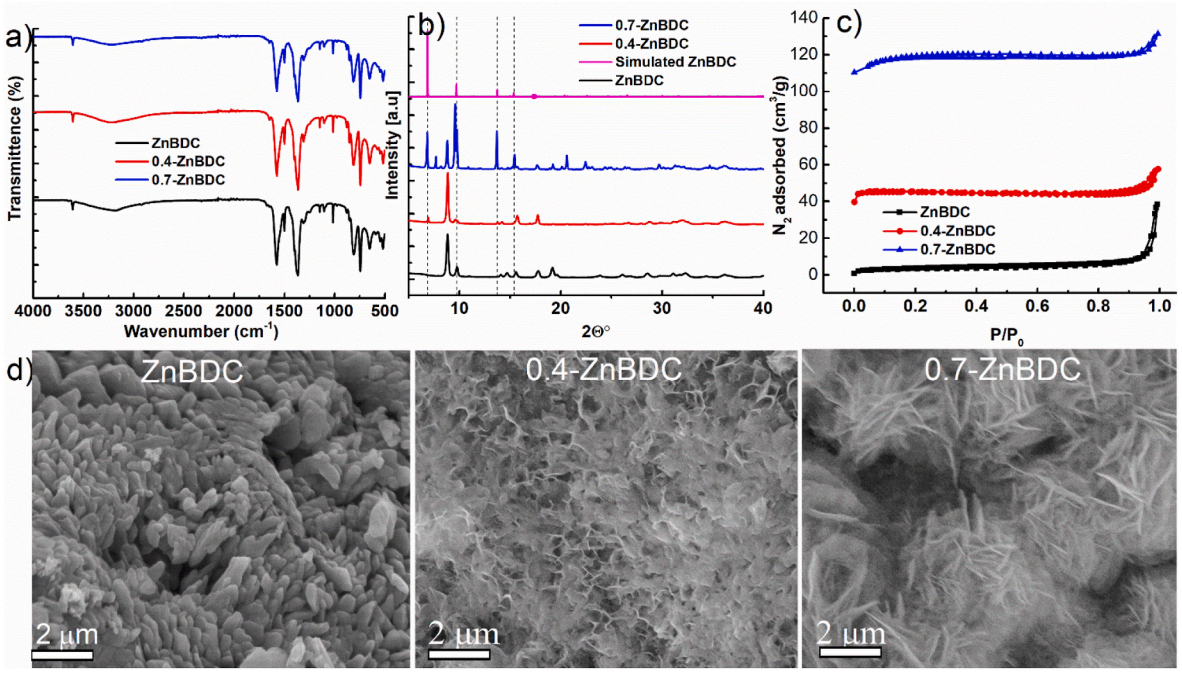

Fig. 2. Characterization of the synthesized Zn(BDC) MOFs using: (a) FTIR, (b) XRD, (c) nitrogen adsorption–desorption isotherms, and (d) SEM imaging.

both the 0.4–Zn(BDC) and 0.7–Zn(BDC) MOFs. The morphology is different from that previously reported literature without the addition of ammonium hydroxide, as the material has now been transformed into thin flakes and sheets. Fig. 2d clearly depicts the layered nanosheet-like structures for both representative samples [32]. The distinctive layered texture was more evident in 0.7–Zn(BDC) compared to 0.4–Zn(BDC), which supports the aforementioned role of NH_4OH towards the formation of a more well-defined morphology.

Different morphologies have been reported in previous studies as a result of solvent modulation, additions of precursors, and/or template assisted synthesis techniques [36–39]. Such morphological changes can play a significant role in the performance of MOFs for different applications, particularly upon transformation to thin sheets and/or flakes, resulting in reduced mass and electron transport resistance [40,41]. Specifically, the morphology and topology of MOFs can be tuned by the addition of NH_4OH. Recently, different morphologies of Cu-based MOFs were reported by the addition of a small amount of NH_4OH in a one-pot synthesis [42]. The change in morphology can be attributed to the formation of a sterically less-hindered zinc complex with ammonium and the high solubility of the organic ligand at high pH in the presence of NH_4OH. The morphology of 0.7–Zn(BDC) was transformed from a nodular structure to well-defined sheets. Such a transformation of 0.7–Zn(BDC) into thin sheets may contribute to the enhanced electrical conductivity [42]. The distribution of zinc in 0.4–Zn/GCE and 0.7–Zn/GCE was verified through SEM/EDX (see Figure S1) by selecting a larger area of the samples. While the distribution of Zn seems similar in both, smoother and thinner sheets, with some discreet particles, can be seen for 0.7–Zn/GCE compared to the more course sheets/particles for 0.4–Zn/GCE. Moreover, the nitrogen adsorption-desorption isotherms (Fig. 2c) showed a high surface area for pristine ZnBDC, 0.4–Zn(BDC) and 0.7–Zn(BDC) samples. The lowest surface area and single point pore volume i.e. 45 m^2/g and 0.06 cm^3/g is observed for pristine Zn(BDC) sample while surface area and single point pore volume is highest for the 0.7–Zn(BDC) sample. Specifically, the BET surface area of 0.7–Zn(BDC) is 500 m^2/g compared to 190 m^2/g for 0.4–Zn(BDC), and the single point pore volume is 0.1 and 0.2 cm^3/g for 0.4–Zn(BDC) and 0.7–Zn (BDC) MOFs, respectively. Such a high surface area and pore size plays a significant role in the enhanced electrochemical performance. It is important to note that the surface area of the MOF sheets decreased due to a change from 3D to 2D structures, however, the electrical conductivity and mechanical properties can still be improved despite their lower surface area [43].

3.2. Electrochemical behaviour of Zn(BDC) based sensors towards TNT

The two modified electrodes (0.4–Zn/GCE and 0.7–Zn/GCE) were prepared as films on a polished GCE substrate for the electrochemical sensing of TNT. Cyclic voltammetry (CV) was employed and the resulting voltammograms are shown in Fig. 3, with the corresponding

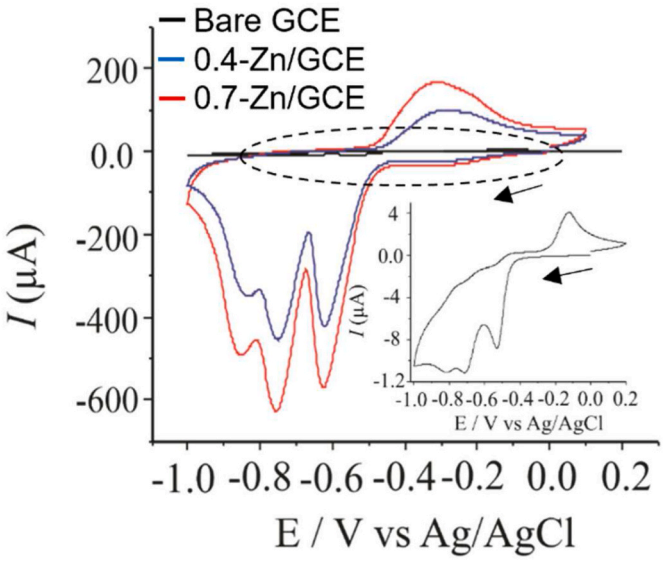

Fig. 3. Superimposed cyclic voltammograms of 0.4–Zn/GCE (red) and 0.7–Zn/GCE (blue) modified GCEs compared to the unmodified (bare) GCE in 0.5 M borate buffered Na_2SO_4 solution at pH 7. The inset shows a magnified image of the CV on the bare GCE. The corresponding blank experiments (in the absence of TNT) are shown in Figure S2 in the supporting information. (For interpretation of the references to colour in this figure legend, the reader is referred to the Web version of this article.)

blank scans in the absence of TNT shown in the supporting information (Figure S2). The pristine (unmodulated) Zn(BDC) sample was also tested in the film, but showed lower current responses compared to the two solvent modulated materials (see Figure S3), so was not studied further.

The electrochemical reduction of TNT in aqueous media is well-studied mechanism, displaying three distinct reduction peaks in the CV attributed to the stepwise reduction of three aromatic nitro groups into amino groups (Fig. 1) [44,45]. Typically, this corresponds to a $6e^-$ and $6H^+$ transfer reaction for each nitro ($–NO_2$) group with the incoming protons from the solvent, making it a total $18e^-$ transfer process [8]. Among the three $–NO_2$ groups, the most conventional reduction pathway starts from one *ortho* group followed by the second *ortho* group then the *para* $–NO_2$ group [8,46]. In this work, the reduction current of the first peak will be analysed for sensing purposes.

The voltammetry of the unmodified GCE towards the electrochemical detection of TNT (0.04 mM) in borate buffered Na_2SO_4 solution at pH 7 and within a potential window of −1.0 to +0.2 V was also studied (Fig. 3 inset). Fig. 3 shows a comparison of the reduction of TNT on a bare GCE and a Zn(BDC) modified GCE, in which the former showed a much smaller current response (−8.8 μA, E_{red} = −0.53 V) compared to the later (−423 and −568 μA for 0.4– and 0.7–Zn(BDC), respectively, E_{red} = – 0.622 V). The higher current for the 0.7–Zn/GCE compared to the 0.4–Zn/GCE is attributed to its well-defined morphology, higher surface area and larger porosity (Fig. 2).

The electrochemical response of the blank (carbon black + Nafion) modified GCE was also examined. This film was prepared in the same way as described in the experimental section, except that the Zn(BDC) MOF was not added. A very weak signal was observed (Fig. 4, black line) compared to the 0.7–Zn/GCE modified electrode, (red line) confirming the exclusive contribution of the employed MOFs towards the detection of TNT.

3.3. Stability of the MOF modified electrodes

To determine the stability and reproducibility of the reported sensor, both the 0.4–(BDC) and 0.7–Zn(BDC) modified GCEs were subjected to repeated CV scans in 0.04 mM TNT solution with 20 and 60 min wait time between each scan, as shown in Figure S4. Employing different wait times ensured that there was enough time for the modified film to recover from the previous cycle, and to examine its stability under prolonged cycling and storage. To ensure consistency, electrode positions were fixed across all measurements. As seen in Figure S4, there was only a very small variation in the peak currents using different wait times, indicating that 20 min is sufficient to maintain a stable current. For the experiments with longer wait times, the electrodes remained dipped into the electrolyte solution over a period of 10 h without any visible fall-off of the active material (MOF) film or any significant drop in current signal. These experiments also revealed the distinct reduction signals of TNT (0.04 mM, first peak at −0.622V) for both modified GCEs, which shows the impressive ability of MOFs to remain electroactive even for long periods of time. Slightly better current stability for the three peaks of TNT on the 0.7–Zn/GCE compared 0.4–Zn/GCE is ascribed to its layered morphology (Fig. 2d), more homogeneous suspension (estimated by visual inspection), and higher surface area, porosity and roughness.

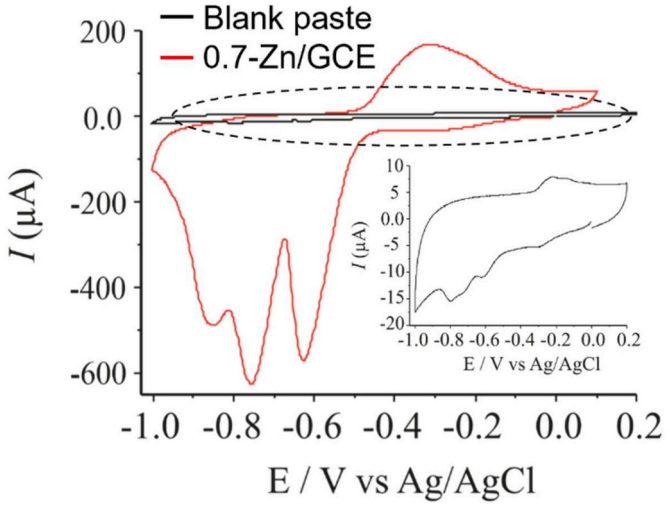

Fig. 4. Superimposed cyclic voltammograms (CVs) of the blank paste (black line, carbon black + Nafion) and 0.7–Zn/GCE (red) modified electrodes in 0.5 M borate buffered Na_2SO_4 solution at pH 7 with 0.04 mM TNT and scan rate of 100 mVs^{-1}. The inset shows the magnified image of the CV of the blank paste. (For interpretation of the references to colour in this figure legend, the reader is referred to the Web version of this article.)

3.4. Impact of pH and scan rate

The pH of the electrolyte is known have substantial impact on the electro-reduction signal of TNT [46]. Indeed, the reduction of TNT involves the formation of radicals and the consumption of several (up to 18) protons, thus the reaction is typically highly sensitive to variations in local pH. Three electrolyte pH values were selected: 4 (slightly acidic), 7 (neutral) and 9 (slightly basic) (Fig. 5. Interestingly, there was very little change in potential of the first reduction peak upon changing pH (less than 30 mV variation across all pH values), whereas ~300 mV shift was observed for a conventional redox probe, hydroquinone (see Figure S5 in the supporting information), using the same MOF modified electrodes. This could indicate an interaction of the MOF with the TNT structure that causes an almost pH independent reduction reaction, which is worthy of a follow-up study in the future. From an analytical perspective, the peak heights also changed with pH, which could be assigned to the involvement of hydronium ions during the reduction of compounds with nitro moieties [47]. The signals with lowest currents were obtained in basic media (pH 9). The most desirable feature for sensing applications (highest TNT current, moderate reduction potential) was obtained at pH 7, so therefore this electrolyte was selected for further measurements. Borate buffered Na_2SO_4 (0.5 M) was used as a supporting electrolyte based on previously reported works, claiming its ability to retain the morphology of Zn based nanostructures [48,49]. For verification of the stability of the complex, the 0.7–Zn(BDC) powder was

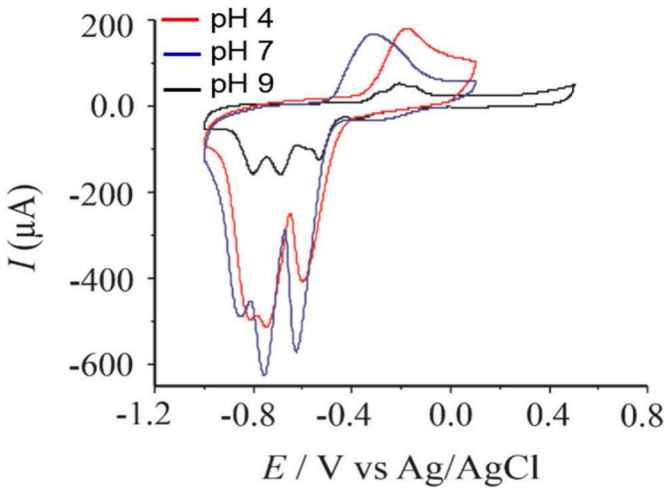

Fig. 5. Superimposed cyclic voltammograms (CVs) of a 0.7–Zn/GCE modified electrode at pH values of 4 (red), 7 (blue) and 9 (black) in 0.5 M borate buffered Na_2SO_4 solution with 0.04 mM TNT and scan rate of 100 mVs^{-1}. (For interpretation of the references to colour in this figure legend, the reader is referred to the Web version of this article.)

soaked in the electrolyte solution for 6 h before collecting SEM images (Figure S6), which did not display any significant changes compared to the original powder.

The dependence of scan rate (ν) on the reduction peak current (I_{pc}) of TNT was investigated in the range of 10–1000 mVs^{-1} for the 0.7–Zn/GCE modified electrode. The recorded voltammograms are presented in Figure S7, which clearly show an increase in current signal with an increase in ν. With increasing ν, a shift in the reduction peak towards a more negative potential was observed, which suggests some electrochemical quasi-reversibility for the reduction of the nitro compound. This behaviour was observed on both the 0.4–Zn/GCE and 0.7–Zn/GCE modified electrodes. The linear correlation between the square root of the scan rate and I_{pc} suggests that the electro-reduction of TNT on both 0.4–Zn/GCE ($R^2 = 0.9852$) and 0.7–Zn/GCE ($R^2 = 0.9854$) modified electrodes is a diffusion controlled process (Figure S8).

3.5. Electrochemical detection of TNT on 0.4–Zn/GCE and 0.7–Zn/GCE

For analytical evaluation of the devised sensor, square wave voltammetry (SWV) was used as a sensing technique due to its higher sensitivity compared to cyclic voltammetry. Quantification was performed on the 0.4–Zn/GCE and 0.7–Zn/GCE modified electrodes under optimized conditions (see experimental section) in 0.5 M borate buffered Na_2SO_4 solution at pH 7. Using a spiking method, SWV was carried out in the range 0.3 μM–1.0 μM. The obtained SWV curves in the cathodic potential range are shown in Fig. 6a and b for 0.4–Zn/GCE and 0.7–Zn/GCE modified electrodes, respectively. To maintain consistency between the CV and SWV measurements, a 20 min wait time was allowed between each scan. The selection of 20 min wait time for the recovery of the sensor was based on our earlier study on ZnO based sensors for methyl paraben detection [50]. To verify the wait time for the sensors in the current study, further tests were performed with wait times of 2 min–10 min for the 0.4–Zn/GCE MOF. It was seen that a wait time of 10 min (see Figure S9) is sufficient to almost recover the response of TNT sensor fully, but 20 min was used in the experiments to ensure full recovery. Three well-separated peaks for TNT were evident in the 0.7–Zn/GCE voltammograms i.e., Fig. 6b at −0.57, −0.69 and −0.79 V. Contrary to this, only two prominent reduction peaks were observed (first two peaks were overlapping and not well resolved) at −0.57 and −0.69 V on the 0.4–Zn/GCE (Fig. 6a).

The current for the first reduction peak at −0.57 V was measured to plot calibration graphs for both the 0.4–Zn/GCE and 0.7–Zn/GCE modified electrodes in the selected concentration range of 0.5–1.0 μM. The first reduction peak displayed excellent linearity compared to the other peaks. The corresponding calibration curves (Fig. 6c and d) for the reduction of TNT were found to be linear in the range of 0.5–1.0 μM for both the 0.4–Zn/GCE and 0.7 Zn/GCE modified electrodes ($R^2 > 0.99$ for both). The limit of detection (LOD) and limit of quantification (LOQ) were calculated by dividing either three or ten times the standard deviation (σ), with the slope of the calibration curve. The calculated LOD values were 0.046 μM and 0.042 μM, and the LOQ values were 0.15 μM and 0.14 μM for the 0.4–Zn/GCE and 0.7–Zn/GCE modified electrodes, respectively. The sensitivities of the modified electrodes were calculated from the calibration curve slopes, and were 106.8 and 87.4 μA/μM for 0.4–Zn/GCE and 0.7–Zn/GCE, respectively. In terms of LOD, our ZnBDC MOF-based sensor performs better than or comparable to the existing literature for TNT sensing on carbon-based electrochemical sensors, e.g. boron doped nanodiamond, carbon nanotubes (CNTs), and even

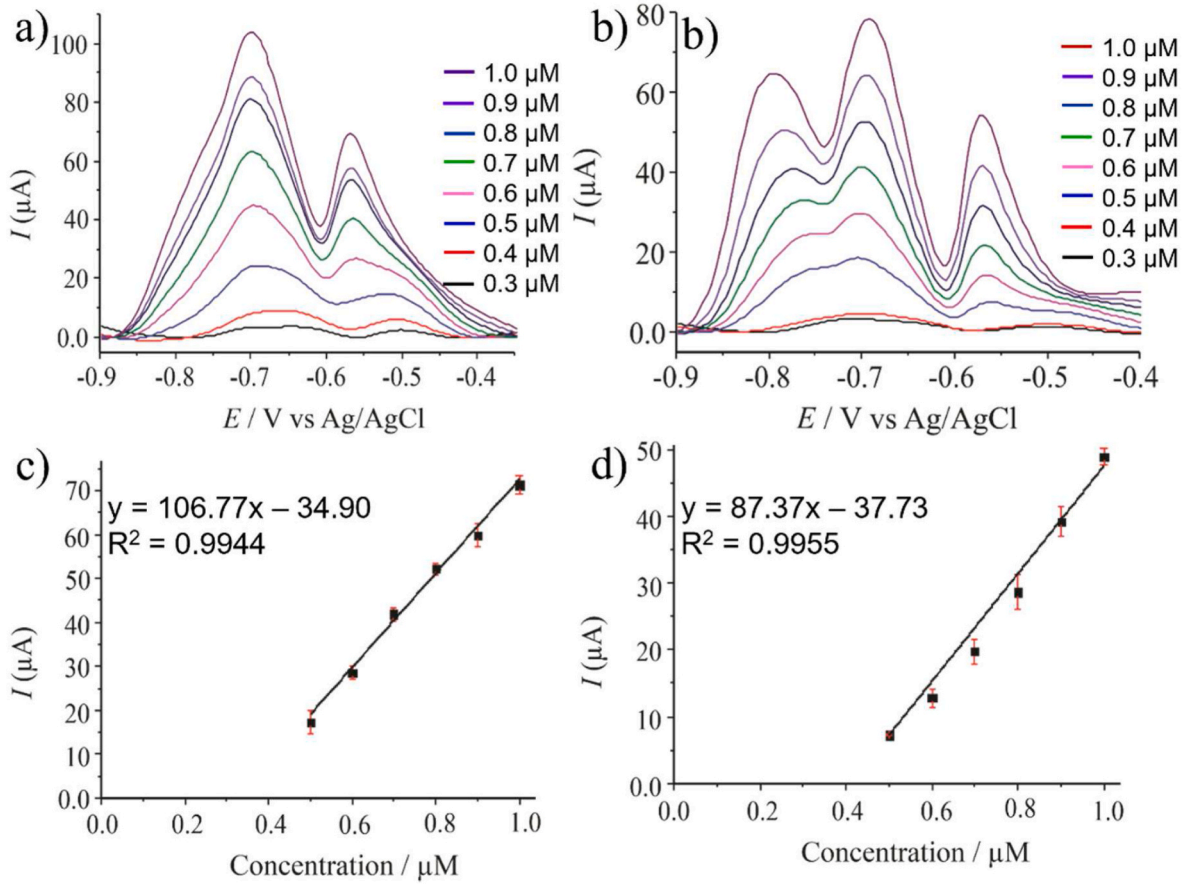

Fig. 6. SWV for (a) 0.4–Zn/GCE and (b) 0.7–Zn/GCE modified electrodes at different concentrations of TNT. Calibration curves from 0.5 to 1.0 μM TNT in 0.5 M borate buffered Na_2SO_4 solution at pH 7 for (c) 0.4–Zn/GCE and (d) 0.7–Zn/GCE. The error bars represent one standard deviation of three repeats on separately prepared electrodes.

precious metals e.g. gold nanoparticles with CNTs (see Table S1 in the supporting information). It is imperative to mention that the LOD in this work for 0.7ZnBDC is 0.042 μM, which is much lower than the benchmark of 0.44 μM for TNT set by the BTAG Freshwater Screening Benchmarks published by the United States Environmental Protection Agency [51].

To demonstrate the reproducibility of the proposed sensor, both modified electrodes were tested with 0.04 mM TNT on three separate electrodes using freshly prepared films. The results demonstrated exceptional reproducibility with a standard deviation of only 1.4 and 0.8% for 0.4–Zn/GCE and 0.7–Zn/GCE, respectively. These results point towards a link between the visually evident more well-defined morphology of the 0.7–Zn/GCE and the better reproducibility and lower LOD towards TNT compared to the 0.4–Zn/GCE. Electrochemical impedance spectroscopy (EIS) was also performed to compare 0.4–Zn/GCE and 0.7–Zn/GCE (see Figure S10). As expected, 0.7–Zn/GCE has lower impedance (49.71 Ω) (Figure S10) compared to 0.4–Zn/GCE (84.47 Ω), which might be attributed to the morphology of thin sheets of the former [42].

3.6. TNT sensing in real water samples

To assess the sensor performance in real matrices, water samples were collected from two different sources: (1) untreated tap water (TW) from the Chemistry & Resources Precincy at Curtin University, Bentley, Perth, Western Australia, and lake water (LW) from Wright lake, Camillo, Western Australia (WA). In this experiment, 0.5 M KCl was added as a supporting electrolyte to provide sufficient conductivity for the measurement. To rule out the presence of interferences, SWV was first carried out in blank TW and LW samples with and without the supporting electrolyte. Fig. 7a shows three well-separated reduction peaks for TNT in LW compared to TW, where the second and third peaks seem to merge closer together. The recorded peak potentials for TNT were also quite different i.e. −0.44 V and −0.58 V vs. Ag/AgCl in LW and TW, respectively. Despite the difference, the results from both real samples clearly suggest the analytical robustness and promising ability of the reported sensor towards the detection of TNT in the presence of a non-toxic and inexpensive electrolyte (KCl).

3.7. Post-characterization of the modified electrode

To gain insights into the preservation of the elemental content and morphology of the MOFs after being subjected to electrochemical sensing experiments for an extended period, further characterization of the materials was performed. Fig. 8 shows scanning electron microscopy (SEM) and elemental maps of the constituent elements obtained for 0.7–Zn(BDC) (a1-a3) in its original form, (b1-b3) before, and (c1-c3) after the extended electrochemical experiments. Comparing Fig. 8 (b1-b3) and (c1-c3) with Fig. 8 (a1-a3) is of prime importance to elaborate on the stability of the Zn(BDC) MOFs after sensing experiments. The existence of constituent elements, especially Zn, supports the fact that the structure of Zn(BDC) remains intact even after performing electrochemical detection experiments for TNT. We note that the carbon and Nafion-containing paste was added to the sample for both the "before" and "after" experimental results, and the lower resolution could result in hazy images due to the high amount of carbon present. High resolution XPS spectra of Zn (Fig. 8 d-f) exhibits two intense peaks at 1022.7 and 1045.8 eV assigned to 2p3/2 and 2p1/2, respectively, which further confirms the retention of the Zn(BDC) structure in its original form [52,53]. The corresponding XPS survey spectra are provided in Figure S11 with the constituent elemental peaks remaining constant. The appearance of sharp fluorine (F) peaks in Figure S11 (b-c) spectra are believed to come from the Nafion used for the ink preparation (see Fig. 9).

To gain atomic-scale insights into the structural and sensing properties of the Zn(BDC) MOF towards trinitrotoluene (TNT), first principles calculations based on spin-polarized density functional theory (DFT) were employed [54,55]. A cubic model system for Zn(BDC) MOF containing 424 atoms ($C_{192}O_{104}H_{96}Zn_{32}$) with an optimized lattice constant of 25.77 Å was considered for the atomistic simulations [56]. The ground state configuration of the bare Zn(BDC) MOF is shown in Fig. 8d. For a more efficient sensing mechanism, Zn(BDC) MOF must bind TNT with a binding that is between strong physisorption and weak chemisorption. This means the calculated binding energy should fall between −0.50 eV and −1.0 eV [57]. In order to find the most stable adsorption configuration of TNT within Zn(BDC), various binding formations were considered by placing the former at different binding sites within the later. On the basis of total energy comparison, the ground state system was found as shown in Fig. 8(a–c). The binding energy (E_b) of TNT with the Zn(BDC) MOF was calculated using the following relationship [35]:

$$E_b = E\,(Zn(BDC)\ @TNT) - E\,(Zn(BDC)) - E\,(TNT) \quad (1)$$

Here, the first, second and third terms on the right-hand side of the above relation represent the total energies (E) of TNT adsorbed on the Zn

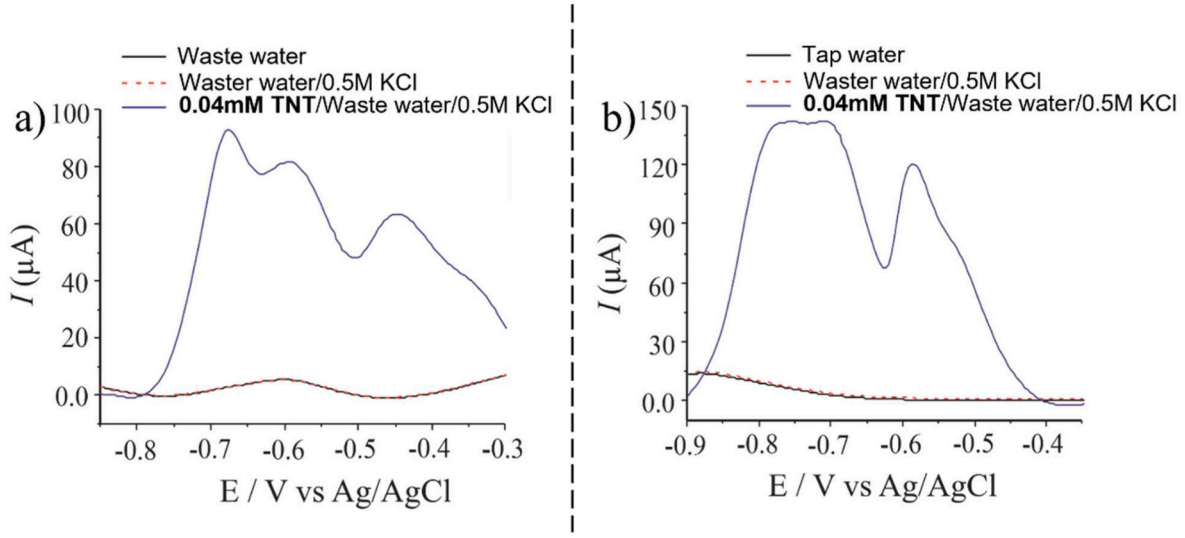

Fig. 7. Superimposed SWV of the 0.7–Zn/GCE modified electrode towards (a) lake water (b) tap water. The water sample contains 0.5 M KCl or 0.5 M KCl spiked with 0.04 mM TNT.

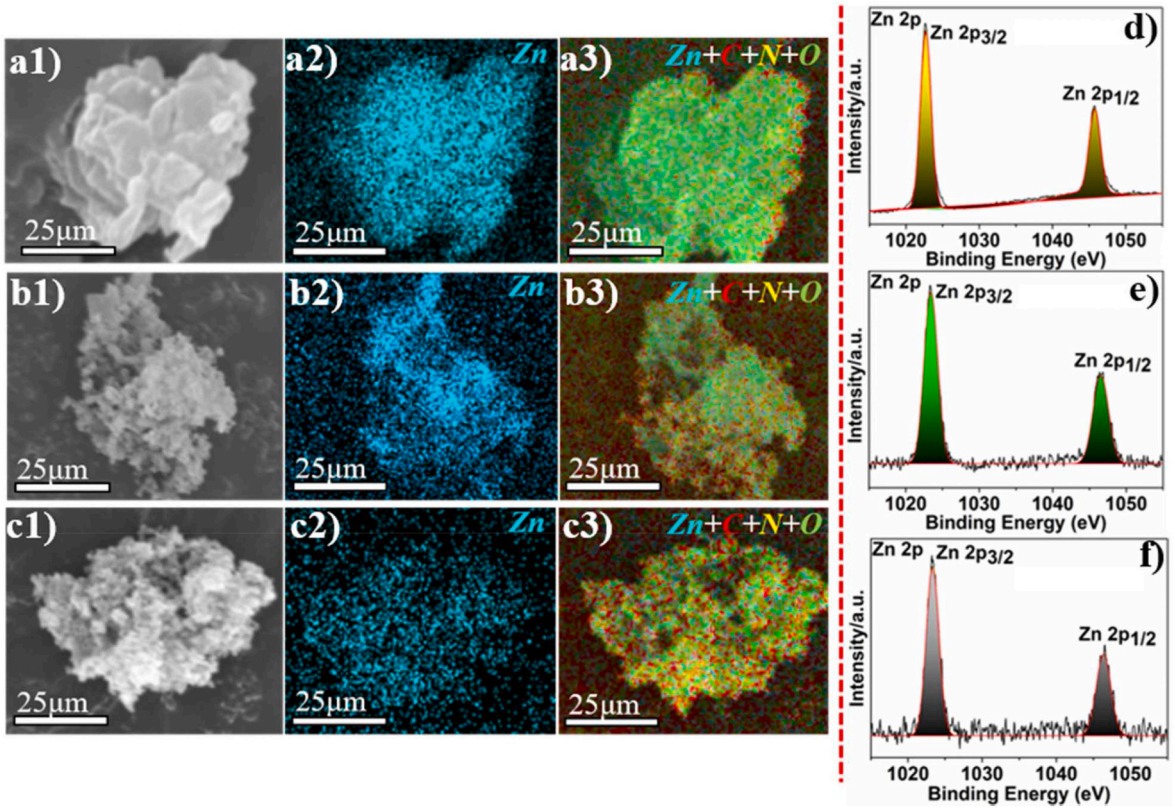

Fig. 8. SEM/EDX of 0.7–Zn(BDC), and high resolution Zn XPS of: (a1-a3) the as prepared 0.7–Zn(BDC), (b1-b3) the 0.7–Zn(BDC) cocktail before experiments, and (c1-c3) the 0.7–Zn(BDC) cocktail after electrochemical detection of TNT. Figures (d–f) show the high resolution XPS spectra of Zn for the three samples.

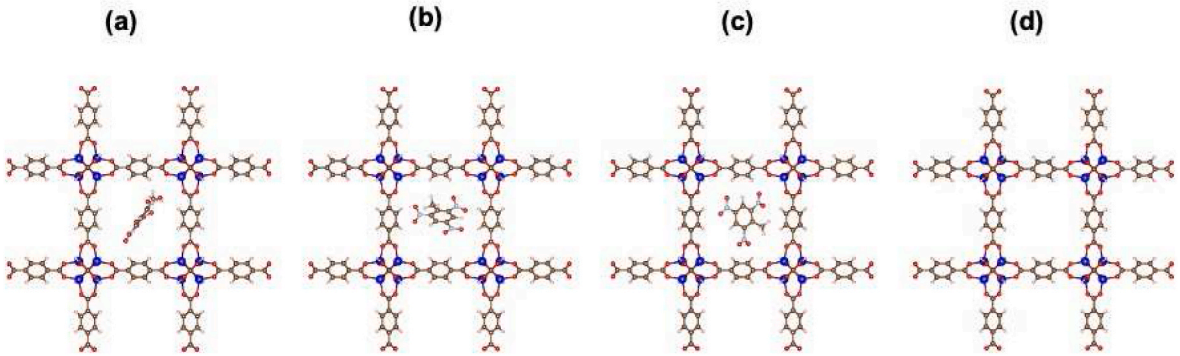

Fig. 9. Optimized computational structures of various orientations (a–c) of TNT adsorbed Zn(BDC) and (d) a bare Zn(BDC). The brown, silver, red, pink, and blue balls represent C, N, O, H, and Zn atoms, respectively. (For interpretation of the references to colour in this figure legend, the reader is referred to the Web version of this article.)

(BDC), the bare Zn(BDC) and the TNT molecule, respectively. The most stable configuration yielded an E_b value of −0.623 eV, which is adequate enough to anchor TNT with Zn(BDC) efficiently. An appropriate E_b value of TNT clearly indicates the promising sensing characteristics of the Zn (BDC) MOF. The TNT molecule aligns itself almost in the centre of the Zn (BDC) with a minimum binding distance between O (TNT) and H (Zn (BDC)) of 3.73 Å in the most stable configuration.

4. Conclusions

Two NH_4OH sensitized Zn(BDC) MOFs were synthesized by using a facile hydrothermal approach and were employed as electrode materials for the voltammetric sensing of the explosive TNT. A higher concentration of NH_4OH (sensitizing agent) during the synthesis leads to the formation of more well-defined structures. The prepared MOFs were used to construct a modified GCE surface for the detection of TNT. Under optimized conditions, improved electrochemical sensing signals could be associated with the different morphology of the MOFs under investigation. The 0.7–Zn(BDC) MOF modified GCE exhibited higher stability and reproducibility as compared to the 0.4–Zn(BDC) MOF. First principles DFT calculations revealed the efficient binding mechanism of Zn (BDC) MOF towards TNT. Besides its excellent performance, the successful response of the electrodes in real spiked water samples shows the possibility of the devised sensor materials for the effective sensing of TNT close to explosion sites for remediation purposes.

Credit author statement

Shaghraf Javaid: Conceptualization, Validation, Formal analysis, Investigation, Writing – original draft, Writing – review & editing. Muhammad Rizwan Azhar: Conceptualization, Validation, Formal analysis, Investigation, Writing – original draft, Writing – review & editing. Xinyu Li: Validation, Investigation, Formal analysis. Juliette I. Phillips: Validation, Investigation, Formal analysis. Tanveer Hussain: Methodology, Investigation, Formal analysis, Writing – original draft. Hussein Abid: Validation. Jun Chen: Methodology, Validation, Investigation, Formal analysis. Xiaobo Ji: Supervision, Funding acquisition. Debbie S. Silvester: Conceptualization, Formal analysis, Writing – review & editing, Supervision, Project administration, Funding acquisition.

Declaration of competing interest

The authors declare that they have no known competing financial interests or personal relationships that could have appeared to influence the work reported in this paper.

Data availability

Data will be made available on request.

Acknowledgements

This work was supported by Cooperative Research Centre for Contamination Assessment and Remediation of the Environment (CRC CARE) (Project No: 2.1.12–19/20). DSS thanks the Australian Research Council (ARC) for a Future Fellowship (FT170100315). The authors thank Natasha Hoffman for performing some experiments at different pH values with the MOF modified electrodes for benzoquinone. The authors acknowledge the facilities and technical assistance of both the X-ray Diffraction & Scattering, and Microscopy & Microanalysis Facilities of the John de Laeter Centre at Curtin University.

Appendix A. Supplementary data

Supplementary data to this article can be found online at https://doi.org/10.1016/j.mtchem.2023.101759.

References

[1] W. Zhao, X. Yang, A. Feng, X. Yan, L. Wang, T. Liang, J. Liu, H. Ma, Y. Zhou, Distribution and migration characteristics of dinitrotoluene sulfonates (DNTs) in typical TNT production sites: effects and health risk assessment, J. Environ. Manag. 287 (2021), 112342.
[2] P. Kovacic, R. Somanathan, Nitroaromatic compounds: environmental toxicity, carcinogenicity, mutagenicity, therapy and mechanism, J. Appl. Toxicol. 34 (2014) 810–824.
[3] S. Singh, Sensors–an effective approach for the detection of explosives, J. Hazard Mater. 144 (2007) 15–28.
[4] Environmental Protection Agency, Criteria and Standard Division, Office of Drinking Water, Health Advisory for TNT, Washington, DC, 1989.
[5] H.A. Yu, J. Lee, S.W. Lewis, D.S. Silvester, Detection of 2,4,6-trinitrotoluene using a miniaturized, disposable electrochemical sensor with an ionic liquid gel-polymer electrolyte film, Anal. Chem. 89 (2017) 4729–4736.
[6] J. Lee, D.S. Silvester, Electrochemical detection of explosive compounds in an ionic liquid in mixed environments: influence of oxygen, moisture, and other nitroaromatics on the sensing response, Aust. J. Chem. 72 (2019).
[7] S. Saglam, A. Uzer, E. Ercag, R. Apak, Electrochemical determination of TNT, DNT, RDX, and HMX with gold nanoparticles/poly(carbazole-aniline) film-modified glassy carbon sensor electrodes imprinted for molecular recognition of nitroaromatics and nitramines, Anal. Chem. 90 (2018) 7364–7370.
[8] C.K. Chua, M. Pumera, L. Rulíšek, Reduction pathways of 2,4,6-trinitrotoluene: an electrochemical and theoretical study, J. Phys. Chem. C 116 (2012) 4243–4251.
[9] X. Wang, C. Chi, K. Zhang, Y. Qian, K.M. Gupta, Z. Kang, J. Jiang, D. Zhao, Reversed thermo-switchable molecular sieving membranes composed of two-dimensional metal-organic nanosheets for gas separation, Nat. Commun. 8 (2017), 14460.
[10] J.S. Stefano, A.P. Lima, C.C. Nascentes, S.R. Krzyzaniak, P.A. Mello, J. M. Gonçalves, E.M. Richter, E. Nossol, R.A.A. Munoz, Electrochemical detection of 2,4,6-trinitrotoluene on carbon nanotube modified electrode: effect of acid functionalization, J. Solid State Electrochem. 24 (2019) 121–129.
[11] Y.T. Yew, A. Ambrosi, M. Pumera, Nitroaromatic explosives detection using electrochemically exfoliated graphene, Sci. Rep. 6 (2016), 33276.
[12] S. Tajik, H. Beitollahi, F.G. Nejad, K.O. Kirlikovali, Q. Van Le, H.W. Jang, R. S. Varma, O.K. Farha, M. Shokouhimehr, Recent electrochemical applications of metal–organic framework-based materials, Cryst. Growth Des. 20 (2020) 7034–7064.
[13] S. Tajik, H. Beitollahi, F. Garkani Nejad, I. Sheikhshoaie, A.S. Nugraha, H.W. Jang, Y. Yamauchi, M. Shokouhimehr, Performance of metal–organic frameworks in the electrochemical sensing of environmental pollutants, J. Mater. Chem. A 9 (2021) 8195–8220.
[14] H. Daglar, S. Keskin, Recent advances, opportunities, and challenges in high-throughput computational screening of MOFs for gas separations, Coord. Chem. Rev. (2020) 422.
[15] H. Fatima, M.R. Azhar, Y. Zhong, Y. Arafat, M. Khiadani, Z. Shao, Rational design of ZnO-zeolite imidazole hybrid nanoparticles with reduced charge recombination for enhanced photocatalysis, J. Colloid Interface Sci. 614 (2022) 538–546.
[16] L. Zhao, X. Duan, M.R. Azhar, H. Sun, X. Fang, S. Wang, Selective adsorption of rare earth ions from aqueous solution on metal-organic framework HKUST-1, J. Adv. Chem. Eng. 1 (2020).
[17] M.R. Azhar, G. Hussain, M.O. Tade, D.S. Silvester, S. Wang, Electrodeposited metal organic framework toward excellent hydrogen sensing in an ionic liquid, ACS Appl. Nano Mater. 3 (2020) 4376–4385.
[18] M.R. Azhar, H.R. Abid, M.O. Tade, V. Periasamy, H. Sun, S. Wang, Cascade applications of robust MIL-96 metal organic frameworks in environmental remediation: proof of concept, Chem. Eng. J. 341 (2018) 262–271.
[19] F. Wang, J. Hu, Y. Liu, G. Yuan, S. Zhang, L. Xu, H. Xue, H. Pang, Turning coordination environment of 2D nickel-based metal-organic frameworks by π-conjugated molecule for enhancing glucose electrochemical sensor performance, Mater. Today Chem. 24 (2022).
[20] Z. Li, M. Song, W. Zhu, W. Zhuang, X. Du, L. Tian, MOF-derived hollow heterostructures for advanced electrocatalysis, Coord. Chem. Rev. 439 (2021).
[21] D.K. Yadav, V. Ganesan, P.K. Sonkar, R. Gupta, P.K. Rastogi, Electrochemical investigation of gold nanoparticles incorporated zinc based metal-organic framework for selective recognition of nitrite and nitrobenzene, Electrochim. Acta 200 (2016) 276–282.
[22] H. Yuan, N. Li, W. Fan, H. Cai, D. Zhao, Metal-organic framework based gas sensors, Adv. Sci. 9 (2022), e2104374.
[23] N. Kajal, V. Singh, R. Gupta, S. Gautam, Metal organic frameworks for electrochemical sensor applications: a review, Environ. Res. 204 (2022), 112320.
[24] H. Wang, S. Jiang, J. Pan, J. Lin, J. Wang, M. Li, A. Xie, S. Luo, Nanomaterials-based electrochemical sensors for the detection of natural antioxidants in food and biological samples: research progress, Microchim. Acta 189 (2022) 318.
[25] N. Nataraj, T.W. Chen, Z.W. Gan, S.M. Chen, M.R. Hatshan, M.A. Ali, Bifunctional 3D-MOF-based nanoprobes for electrochemical sensing and nanozyme enhanced with peroxidase mimicking for colorimetric detection of acetaminophen, Mater. Today Chem. 23 (2022).
[26] I. Stassen, B. Bueken, H. Reinsch, J.F.M. Oudenhoven, D. Wouters, J. Hajek, V. Van Speybroeck, N. Stock, P.M. Vereecken, R. Van Schaijk, D. De Vos, R. Ameloot, Towards metal-organic framework based field effect chemical sensors: UiO-66-NH2 for nerve agent detection, Chem. Sci. 7 (2016) 5827–5832.
[27] S. Dong, G. Suo, N. Li, Z. Chen, L. Peng, Y. Fu, Q. Yang, T. Huang, A simple strategy to fabricate high sensitive 2,4-dichlorophenol electrochemical sensor based on metal organic framework Cu3(BTC)2, Sens. Act. B 222 (2016) 972–979.
[28] J. Li, J. Xia, F. Zhang, Z. Wang, Q. Liu, A novel electrochemical sensor based on copper-based metal-organic framework for the determination of dopamine, J. Chen. Chem. Soc. 65 (2018) 743–749.
[29] T.T. Minh, N.H. Phong, H. Van Duc, D.Q. Khieu, Microwave synthesis and voltammetric simultaneous determination of paracetamol and caffeine using an MOF-199-based electrode, J. Mater. Sci. 53 (2017) 2453–2471.
[30] A. Umemura, S. Diring, S. Furukawa, H. Uehara, T. Tsuruoka, S. Kitagawa, Morphology design of porous coordination polymer crystals by coordination modulation, J. Am. Chem. Soc. 133 (2011) 15506–15513.
[31] H.R. Abid, H.M. Ang, S. Wang, Effects of ammonium hydroxide on the structure and gas adsorption of nanosized Zr-MOFs (UiO-66), Nanoscale 4 (2012) 3089–3094.
[32] Y. Lv, S. Wang, R. Zhang, D. Zhang, H. Yu, G. Lu, PH-modulated formation of uniform MOF-5 sheets, Inorg. Chem. Commun. 97 (2018) 30–33.
[33] L.Á. Alfonso Herrera, P.K. Camarillo Reyes, A.M. Huerta Flores, L.T. Martínez, J. M. Rivera Villanueva, BDC-Zn MOF sensitization by MO/MB adsorption for photocatalytic hydrogen evolution under solar light, Mater. Sci. Semicond. Process. 109 (2020).
[34] D.K. Yadav, V. Ganesan, F. Marken, R. Gupta, P.K. Sonkar, Metal@MOF materials in electroanalysis: silver-enhanced oxidation reactivity towards nitrophenols adsorbed into a zinc metal organic framework—Ag@MOF-5(Zn), Electrochim. Acta 219 (2016) 482–491.
[35] N. Lock, Y. Wu, M. Christensen, L.J. Cameron, V.K. Peterson, A.J. Bridgeman, C. J. Kepert, B.B. Iversen, Elucidating negative thermal expansion in MOF-5, J. Phys. Chem. C 114 (2010) 16181–16186.
[36] S. Song, X. Ma, W. Li, B. Zhang, J. Sun, C. Deng, The influence of solvent controlled morphology on capacitive properties of metal-organic frameworks based on polyaminocarboxybenzene ligands, Colloids Surf., A (2023) 656.

[37] J. Park, J.Y. Koo, H.C. Choi, The solvent influenced coordination variation of flexible ligands to Y(iii) towards MOF structural diversity, CrystEngComm 24 (2022) 846–853.
[38] N. Al Amery, H.R. Abid, S. Al-Saadi, S. Wang, S. Liu, Facile directions for synthesis, modification and activation of MOFs, Mater. Today Chem. 17 (2020).
[39] C. Fan, Y. Luo, Y. Song, T. Xu, X. Zhang, Microscale synthesis system for regulation and prediction of metal organic framework morphologies, Mater. Today Chem. 23 (2022).
[40] N. Zhou, F. Su, C. Guo, L. He, Z. Jia, M. Wang, Q. Jia, Z. Zhang, S. Lu, Two-dimensional oriented growth of Zn-MOF-on-Zr-MOF architecture: a highly sensitive and selective platform for detecting cancer markers, Biosens. Bioelectron. 123 (2019) 51–58.
[41] A.S. Morshedy, H.M. Abd El Salam, A.M.A. El Naggar, T. Zaki, Hydrogen production and in situ storage through process of water splitting using mono/binary metal–organic framework (MOF) structures as new chief photocatalysts, Energy Fuel. 34 (2020) 11660–11669.
[42] M. Qi, Y. Zhou, Y. Lv, W. Chen, X. Su, T. Zhang, G. Xing, G. Xu, O. Terasaki, L. Chen, Direct construction of 2D conductive metal-organic frameworks from a nonplanar ligand: in situ scholl reaction and topological modulation, J. Am. Chem. Soc. 145 (2023) 2739–2744.
[43] G. Chakraborty, I.H. Park, R. Medishetty, J.J. Vittal, Two-Dimensional metal-organic framework materials: synthesis, structures, properties and applications, Chem. Rev. 121 (2021) 3751–3891.
[44] H.A. Yu, D.A. DeTata, S.W. Lewis, D.S. Silvester, Recent developments in the electrochemical detection of explosives: towards field-deployable devices for forensic science, Trends Anal. Chem. 97 (2017) 374–384.
[45] J. Wang, Electrochemical sensing of explosives, Electroanalysis 19 (2007) 415–423.
[46] A. Dettlaff, P. Jakobczyk, M. Ficek, B. Wilk, M. Szala, J. Wojtas, T. Ossowski, R. Bogdanowicz, Electrochemical determination of nitroaromatic explosives at boron-doped diamond/graphene nanowall electrodes: 2,4,6-trinitrotoluene and 2,4,6-trinitroanisole in liquid effluents, J. Hazard Mater. 387 (2020), 121672.
[47] C.K. Chua, M. Pumera, Influence of methyl substituent position on redox properties of nitroaromatics related to 2,4,6-trinitrotoluene, Electroanalysis 23 (2011) 2350–2356.
[48] V.M. Sofianos, J. Lee, D.S. Silvester, P.K. Samanta, M. Paskevicius, N.J. English, C. E. Buckley, Diverse morphologies of zinc oxide nanoparticles and their electrocatalytic performance in hydrogen production, J. Energy Chem. 56 (2021) 162–170.
[49] C.F. Liu, Y.J. Lu, C.C. Hu, Effects of anions and pH on the stability of ZnO nanorods for photoelectrochemical water splitting, ACS Omega 3 (2018) 3429–3439.
[50] S. Javaid, J. Lee, M.V. Sofianos, Z. Douglas-Moore, D.W.M. Arrigan, D.S. Silvester, Zinc oxide nanoparticles as antifouling materials for the electrochemical detection of methylparaben, Chemelectrochem 8 (2021) 187–194.
[51] EPA freshwater screening benchmarks. https://www.epa.gov/risk/freshwater-screening-benchmarks, Accessed July 2023.
[52] R. Dutta, M.N. Rao, A. Kumar, Investigation of ionic liquid interaction with ZnBDC-metal organic framework through scanning EXAFS and inelastic neutron scattering, Sci. Rep. 9 (2019), 14741.
[53] A.C. Elder, S. Bhattacharyya, S. Nair, T.M. Orlando, Reactive adsorption of humid SO2 on metal–organic framework nanosheets, J. Phys. Chem. C 122 (2018) 10413–10422.
[54] G. Kresse, J. Hafner, Ab initio molecular-dynamics simulation of the liquid-metal–amorphous-semiconductor transition in germanium, Phys. Rev. B 49 (1994) 14251–14269.
[55] G. Kresse, J. Hafner, Ab initio molecular dynamics for liquid metals, Phys. Rev. B 47 (1993) 558–561.
[56] B. Civalleri, F. Napoli, Y. Noël, C. Roetti, R. Dovesi, Ab-initio prediction of materials properties with CRYSTAL: MOF-5 as a case study, CrystEngComm 8 (2006) 364–371.
[57] B. Huang, Z. Li, Z. Liu, G. Zhou, S. Hao, J. Wu, B.-L. Gu, W. Duan, Adsorption of gas molecules on graphene nanoribbons and its implication for nanoscale molecule sensor, J. Phys. Chem. C 112 (2008) 13442–13446.